Fatigue & Fracture of
Engineering Materials & Structures

doi: 10.1111/j.1460-2695.2010.01457.x

Numerical and experimental investigation of mixed-mode fracture parameters on silicon nitride using the Brazilian disc test

G. LEVESQUE[1], N. K. ARAKERE[1], J. J. MECHOLSKY[2] and K. GOPALAKRISHNAN[2]

[1]*Department of Mechanical and Aerospace Engineering, University of Florida, Gainesville, FL 32611, USA,* [2]*Department of Materials Science, University of Florida, Gainesville, FL 32611, USA*

Received in final form 22 February 2010

ABSTRACT Engineering applications of ceramics can often involve mixed-mode conditions involving both tensile and shear loading. Mixed-mode fracture toughness parameters are evaluated for applicability to ceramics using the Brazilian disc test on silicon nitride. Semi-elliptical centrally located surface flaws are induced on the disc specimens using Vickers indentation and compression loaded to fracture with varying levels of mode mixity. The disc specimens are modelled via 3D finite element analysis and all three modes of stress intensity factors computed along the crack front, at failure load. We present a numerical and experimental investigation of four widely used mixed-mode fracture criteria and conclude that the critical strain energy release rate criterion is simple to implement and effective for silicon nitride under mixed-mode conditions.

Keywords Brazilian disc test; brittle fracture; fracture toughness; mixed-mode fracture; silicon nitride.

NOMENCLATURE

a = semi-elliptical crack depth
b = semi-elliptical crack semi-width
B = disc specimen thickness
c = disc half-width
c_v = distance from centre of indent to crack tip
D = disc specimen width
E = Young's modulus
H = hardness
K_c = fracture toughness
K_{I} = opening-mode stress intensity factor
K_{II} = sliding-mode stress intensity factor
K_{III} = shearing-mode stress intensity factor
P = total applied load to the disc
$r_1 = r_1^2 = (R-y)^2 + x^2$
$r_2 = r_2^2 = (R+y)^2 + x^2$
S = strain energy density factor
S_1, S_2, S_3 = specimen number
Y_1 = geometric constant for opening mode empirical K_I equation
Y_2 = geometric constant for sliding mode empirical K_{II} equation
μ = shear modulus, $\mu = E/2\,(1+\nu)$
$\eta = \eta = (3-\nu)/1+\nu$ *(plane stress state)*, $\eta = 3 - 4\nu$ *(plane strain state)*
θ = angle of crack with respect to the load axis

Correspondence: N. K. Arakere. E-mail: nagaraj@ufl.edu

σ = stress
σ_{std} = standard deviation
γ = angle between the initial crack plane and the plane of propagation

INTRODUCTION

Ceramic components in engineering applications can often be subjected to conditions of tensile and shear loading. Silicon nitride balls used in hybrid bearings are a good example of such an application where the balls are subjected to Hertzian loading leading to compressive and shear traction loading at the contact surface along with tensile stresses that exist at the periphery of the elliptical contact. A complex triaxial stress state is present in the subsurface contact region. Surface flaws on the ball are subjected to complex mixed-mode loading conditions resulting from rolling contact fatigue. Study of mixed-mode fracture of ceramics is of considerable engineering interest. Mixed-mode fracture of brittle materials has been investigated by many researchers for finding a single parameter, K_c, which is effective at determining the mixed-mode fracture toughness of a given material. In reality, there has been much divergence in the equations provided for brittle materials which are often empirical in nature and both material and experiment dependent.[1]

The Brazilian disk (BD) test, first proposed by Carniero and Barcellos in 1953[2] has since been used to measure the tensile strength and fracture toughness of brittle materials like rocks, concrete and ceramics. The BD test consists of a precracked circular disk loaded in compression that results in a tensile stress at the centre (perpendicular to the loading direction) and can split the disk along the load axis.[2] With the crack size visible at the end of the experiment, and the final load to fracture known from the load frame, a fracture toughness can be calculated.[3] The advantage of this test is that it can be performed under a range of mode-mixities (from pure mode I to a mix of mode I and II) to evaluate a mixed-mode fracture toughness along with simple specimen geometry and minimal requirements for implementation. Brazilian disk specimen has also been used to measure interfacial fracture toughness in biomaterials.[4] There are two approaches for producing pre-cracks in a specimen, (i) from surface flaws produced by indentations (where small flaws are needed for brittle materials) and (ii) by using the chevron notch, for larger through-thickness cracks for materials with stable crack growth during the initial pre-cracking. For silicon nitride, because the material is brittle and very difficult to cut or grind, surface flaws via indentation is the preferred approach.

There have been quite a number of studies conducted on mixed-mode fracture toughness via multiple approaches on a variety of materials. Zhou *et al.* tested Polymethylmethacrylate (PMMA) with a chevron notch to determine its mode I fracture toughness in the BD test.[5] Tong, *et al.* used the Brazilian disk test to determine the interfacial fracture toughness in bone-cement interfaces.[6] Awaji and Sato employed this test for examining the fracture toughness of graphite, plaster and marble in mixed-mode loading using machined central cracks.[7] Petrovic and Mendiratta have examined mixed-mode fracture toughness in hot pressed silicon nitride using controlled surface flaws produced by Knoop indentation in a four-point bending test.[8] Khandelwal, *et al.* have found the high temperature mixed-mode fracture toughness of hot isostically pressed, PY6 silicon nitride using bend bars which contained cracked indentations produced using the Vickers hardness indenter and tested using the four point bend test.[9]

Herein, we implement the BD test to determine mixed-mode fracture toughness of NBD 300 silicon nitride. Motivation for this study is provided by the application of silicon nitride in hybrid ball bearing applications because it has several desirable properties including high hardness, a low coefficient of thermal expansion, corrosion resistance, and a third the density of common bearing metals.[10] However, the material has low fracture toughness of about 6.0 MPa$\sqrt{}$m.[3] In the course of the manufacturing process, silicon nitride balls are subjected to a lapping process, to achieve the final submicron accuracy in ball diameter and circularity, where the balls are susceptible to low-velocity ball collisions. These low velocity interactions induce small surface cracks on the surface of the ball that, under operating conditions in a ball bearing, are subjected to rolling contact fatigue conditions.[11] Under these conditions, crack growth, under mixed-mode loading, can lead to spallation and, as a result, these surface cracks are the biggest contributors to ball (and therefore bearing) failure.[11,12] If finite element analysis (FEA) can simulate these flaws under service conditions, then the nature of the effective crack driving force resulting from stress intensity factors (SIFs) K_I, K_{II} and K_{III} must be properly understood in order to determine whether or not a crack is in the regime of growth. Herein, we focus on defining an effective mixed-mode fracture parameter for silicon nitride.

EXPERIMENTAL PROCEDURE

Brazilian disc NBD 300 silicon nitride specimens are 25.4 mm (1 in.) in diameter and 2 mm thick. They are cut from bar stock and polished to 0.05 μm surface finish. The discs are pre-cracked using a series of collinear Vickers indentations performed on a Zwick Vickers Hardness Testing Machine using 20 kg load such that the penny cracks formed by individual indents link up, to form one long semi-elliptical surface crack, as shown in Fig. 1. The cracks initiated by closely spaced indents are seen to link up and form one large semi-elliptical crack. Multiple indents are used because the load required to propagate a penny crack from a single indent is very high, causing the discs to fracture at the support platens rather than propagate the centre crack. The dimensions of the cracks induced are recorded of Table 1.

With the specimens prepared in this fashion, they are placed into a conformal fixture with the cracks oriented at an acute angle to the load axis as illustrated in Fig. 2. The specimens are then loaded at a rate of 45.4 kg/min (100 lbs/min), because faster loading can result in fracture occurring at the platens instead of growing the created centre crack until fracture and then the test is stopped. Figure 3 shows three fractured BD specimens for different crack angles.

The load at which the specimen cracked and dimensions of the crack are recorded for each specimen at a number of different angles to the load line (see Table 1). This information will be used to calculate SIFs for the specimens at fracture in FEA.

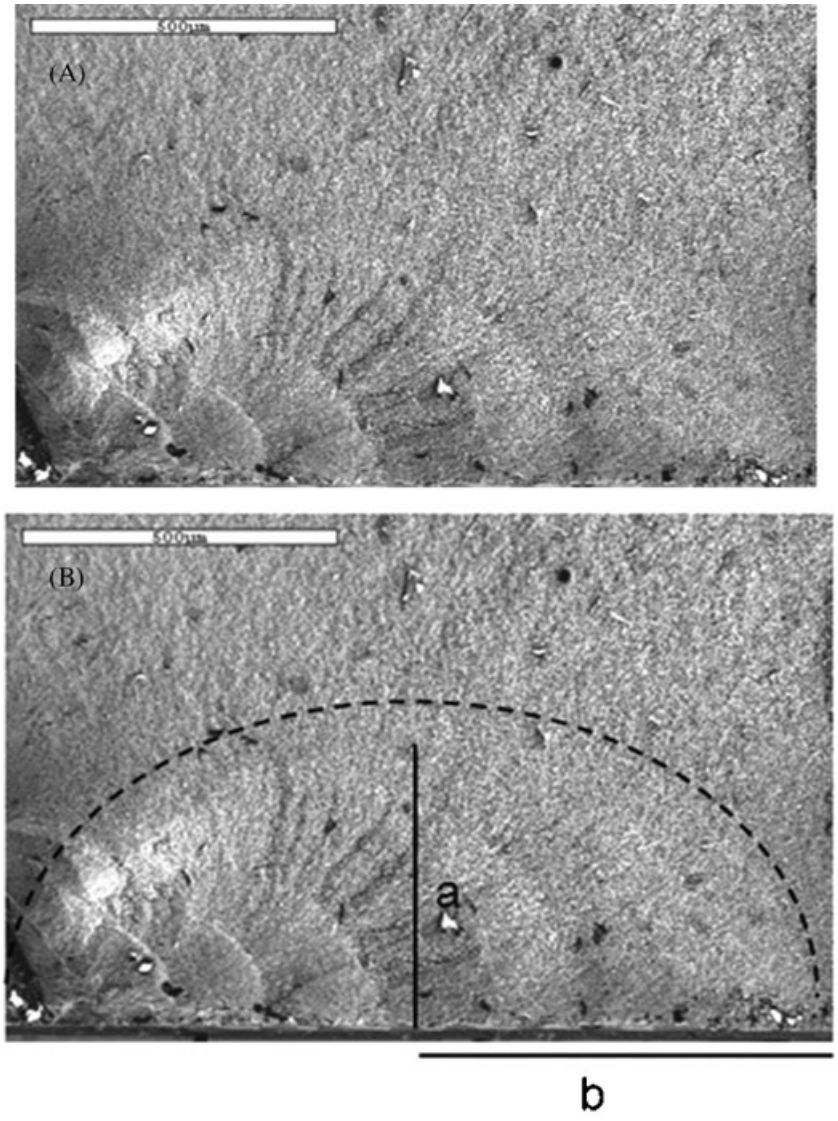

Fig. 1 (A) An example of a fracture surface and (B) with the measured pre-crack dimensions *a* and *b*. Note the semi-elliptical arcs within the crack front indicating linking semi-elliptical cracks from left to right.

Table 1 The sample number, crack turning angle, crack dimensions and fracture load of each specimen examined

θ (°) and Sample	γ (°)	$2b$ (mm)	a (mm)	P (N)
0° S1	0°	3.01	0.26	8940
0° S2	0°	3.10	0.39	7659
10° S1	12°	5.00	0.23	7200
10° S2	18°	2.68	0.49	10640
10° S3	15°	1.94	0.49	9341
20° S1	26°	0.65	0.28	10100
20° S2	28°	0.63	0.23	12342
20° S3	20°	0.50	0.19	13950
30° S1	19°	1.38	0.32	9870
30° S2	21°	2.70	0.44	9010
30° S3	38°	0.49	0.23	14540

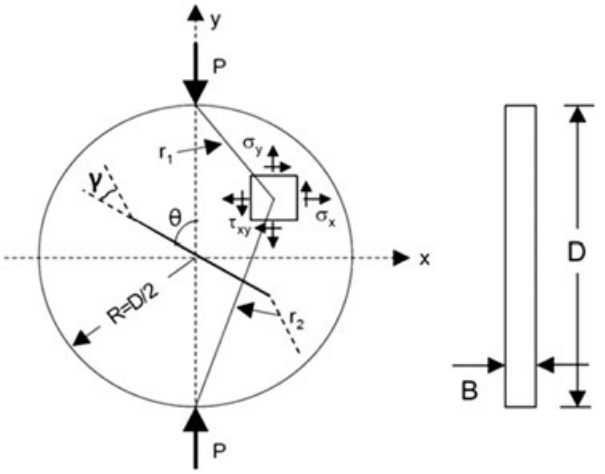

Fig. 2 Schematic showing the flaw orientation on a Brazilian disk specimen as well as the coordinates and components used in the analytical stress equations.

ANALYTICAL EXPRESSIONS FOR MIXED-MODE STRESS INTENSITY FACTORS

Prior research has used the equations for stress intensity factors (SIFs) for small (with respect to the specimen thickness) semicircular flaws (formed by Vickers indentation) loaded under mixed-mode conditions approximated by:[13]

$$K_{\mathrm{I}} = Y_1 \sigma \sqrt{c} \cos^2(\theta) \tag{1}$$

$$K_{\mathrm{II}} = Y_2 \sigma \sqrt{c} \sin\theta \cos\theta, \tag{2}$$

where σ is the applied stress, $c = \sqrt{ab}$ is the equivalent semicircular crack length, a the depth, or the semi-minor, and b is the semi-width, or the semi-major axis dimension, of the elliptical crack. Y_1 and Y_2 are geometric constants equal to 1.65 and 1.55 respectively for indented

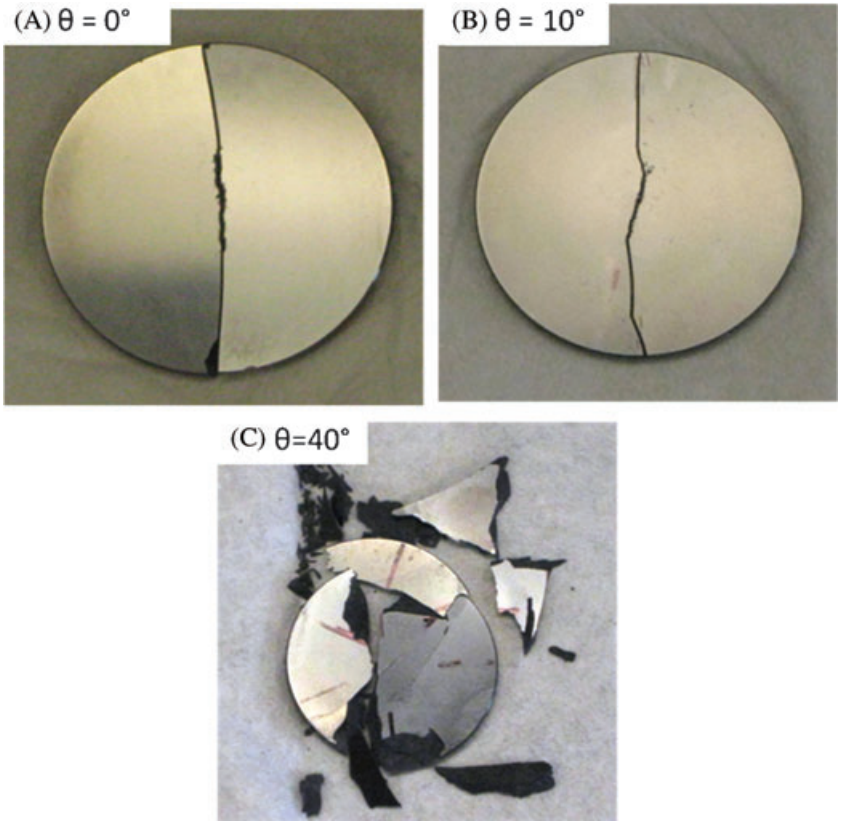

Fig. 3 Examples of cracked BD specimens for the cases of (A) $\theta = 0°$ (B) $\theta = 10°$ and (C) $\theta = 40°$.

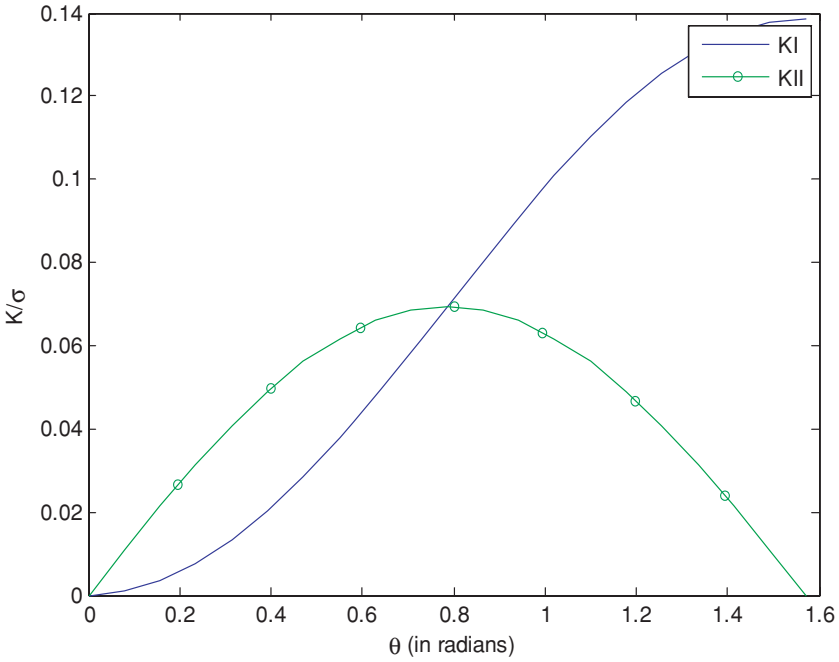

Fig. 4 Non-dimensionalized K_I and K_{II} (with respect to normal and shearing stresses, respectively) from empirical equations for different angles of loading orientation for $b = .02$ m $a = 0.0025$ m.

specimens.[14] These equations were implemented to approximate the SIFs for semi-elliptical flaws from equations for angled through-cracks in a biaxial stress field with a geometric constant. These equations do not discern crack closure and will always give non-zero K_I values (except at $\theta = 0^\circ$) even where experimental observations indicate crack closure at angles above $\sim 35^\circ$. Furthermoore, Eqs (1) and (2), although attributed to a semi-elliptical crack, only give K_I and K_{II} for a single unspecified point along the crack front even though SIFs vary along the crack front and also neglect K_{III}. For $b = 0.02$m and $a = 0.0025$m, K_I and K_{II} are plotted as a function of the angle that the specimen in loaded at in Fig. 4.

STRESS INTENSITY FACTOR COMPUTATION USING 3D FINITE ELEMENT MODELLING

For mixed-mode stress intensity factors for a three dimensional (3D) finite thickness BD specimen with a centre semi-elliptical surface crack, we have to resort to numerical methods. We utilize 3D finite element analysis (FEA) to model each of the cracked specimens under the load which induced cracking to calculate the critical SIFs. The disk is initially modelled uncracked and the stresses at the centre of the disk compared to 2D analytical solution, for model verification. The stresses at the centre of the disc can be calculated according to:[14]

$$\sigma_x(0,0) = \frac{2P}{\pi BD} \tag{3}$$

$$\sigma_y(0,0) = \frac{-6P}{\pi BD} \tag{4}$$

$$\tau_{xy}(0,0) = 0, \tag{5}$$

where y is in the direction of load, P is the applied compressive load, B the specimen thickness, and D is the diameter of the disc and the two-dimensional (2D) plane stress state for an uncracked disc is given by:[14]

$$\sigma_x = -\frac{2P}{\pi B}\left[\frac{(R-y)x^2}{r_1^4} + \frac{(R+y)x^2}{r_2^4} - \frac{1}{2R}\right] \tag{6}$$

$$\sigma_y = -\frac{2P}{\pi B}\left[\frac{(R-y)^3}{r_1^4} + \frac{(R+y)^3}{r_2^4} - \frac{1}{2R}\right] \tag{7}$$

$$\tau_{xy} = \frac{2P}{\pi B}\left[\frac{(R-y)^2 x}{r_1^4} - \frac{(R+y)^2 x}{r_2^4}\right] \tag{8}$$

$$r_1^2 = (R-y)^2 + x^2 \tag{9}$$

$$r_2^2 = (R+y)^2 + x^2, \tag{10}$$

where variables are defined in Fig. 2. The 3D FE model stress results on the mid-plane of the disc showed excellent agreement with the analytical expressions (Eqs 6–8).

The FE mesh for a 3D disc model with a centre crack with varying angles to the load necessitates the use of submodelling. A smaller square submodel, shown in Fig. 5, was used for remeshing cracks of different angles and aspect ratios. The boundaries of this model are displaced according to a submodelling technique, where we apply appropriate displacements to the boundary to simulate it being a part of the larger model.[15] To ensure that

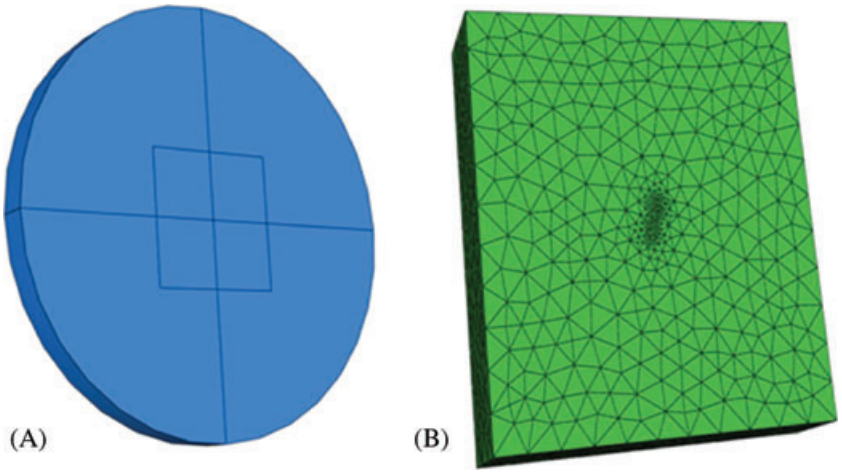

Fig. 5 BD finite element model showing, (A) unmeshed global uncracked model with square partition indicating submodel boundaries and (B) cracked meshed submodel for specimen 2 for $\theta = 20^\circ$.

the boundary of the submodel is sufficiently far away such that the crack presence does not affects its displacements benchmark studies were conducted.

The computation of SIFs involves a two-step process: (i) the meshed cracks are analysed with FRANC3D/NG by $\mathcal{J}$-integral decomposition, because material is still treated as isotropic, though FRANC3D/NG is capable of calculating SIFs in anisotropic materials,[16] and the SIFs are computed as a function of position along the crack front, and not just at one location, as in Eqs (1) and (2), (ii) the contribution to SIFs from residual stresses created by the Vickers indentation are incorporated. The SIFs calculated from the BD FEA simulations cannot include the effects of residual stress induced in the specimen during Vickers indentation. Because this effect can be significant, for point A (in Fig. 6), we superpose the effect of the residual stress on mode I SIF using the well-known equation:[17,18]

$$K_{\mathrm{I}}^{\mathrm{resid}} = 0.016 \left(\frac{E}{H}\right)^{1/2} \left(\frac{P}{c_d^{3/2}}\right), \tag{11}$$

where E is the Young's modulus (310 GPa), H is the hardness (equal to 15.5 GPa according to indentation testing), P is the indentation load (196 kN), and c_d is the distance from the centre of the last indent to the end of the large semi-elliptical crack (here we use 0.47 mm). Using these values we get $K_{\mathrm{I}}^{\mathrm{resid}} = 1.40\ \mathrm{MPa}\sqrt{\mathrm{m}}$. So K_{I} is the result of superposition of mode I SIF contributions due to the stress field from the applied load, computed via FEA, and from the residual stress field:

$$K_{\mathrm{I}} = K_{\mathrm{I}}^{\mathrm{FEA}} + K_{\mathrm{I}}^{\mathrm{resid}}. \tag{12}$$

For crack angle $\theta = 0^\circ$, only mode I SIF is active along the crack front. For $\theta > 0^\circ$ mode mixity along the crack front varies and for the semi-elliptical surface crack analysed mode III component can also be active. Figure 6 shows crack tip displacements as a function of position for $\theta = 20^\circ$, to illustrate the presence of K_{III} at certain locations along the crack front. The K_{III} component is zero for through thickness cracks and is present for semi-elliptical surface cracks at an angle in a BD specimen. We note that while modes I and II are active along the crack front, mode II is highest at the surface (point A) and zero at depth (point B) while mode III is zero at the surface and highest at depth. The distribution of K_{I}, K_{II} and K_{III} along the crack front is shown in Figs 7–9, for several crack angles. These results are discussed in greater detail in the analysis section. On the surface, SIFs can be affected by the residual stresses induced by the Vickers indents but there is no K_{III} component (which is the component that has been investigated the least in prior work). A complete analysis requires 3D FEA and can provide us the advantage of calculating SIFs along the entire crack front.[19] We conduct a systematic analysis to investigate

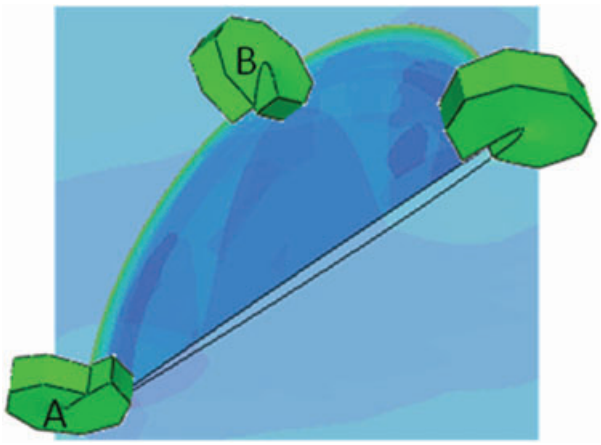

Fig. 6 The displacement field of Sample 1 for $\theta = 20^\circ$, with a scale factor of 100 and translucency applied to view the crack superposed with elements of the circular contour regions to illustrate the presence of K_{II} at the surface and K_{III} at the depth.

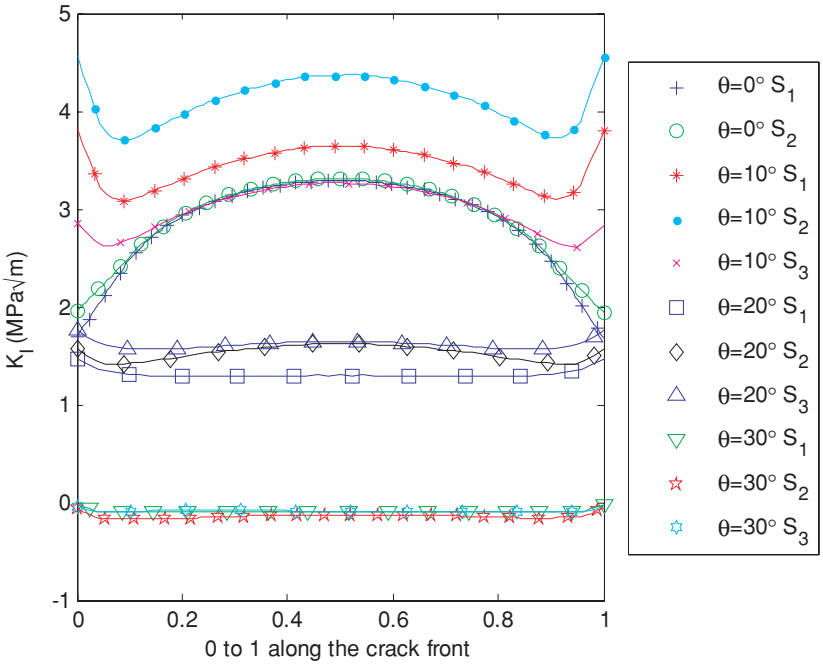

Fig. 7 K_I for all analysed specimens as a function of position along the crack front.

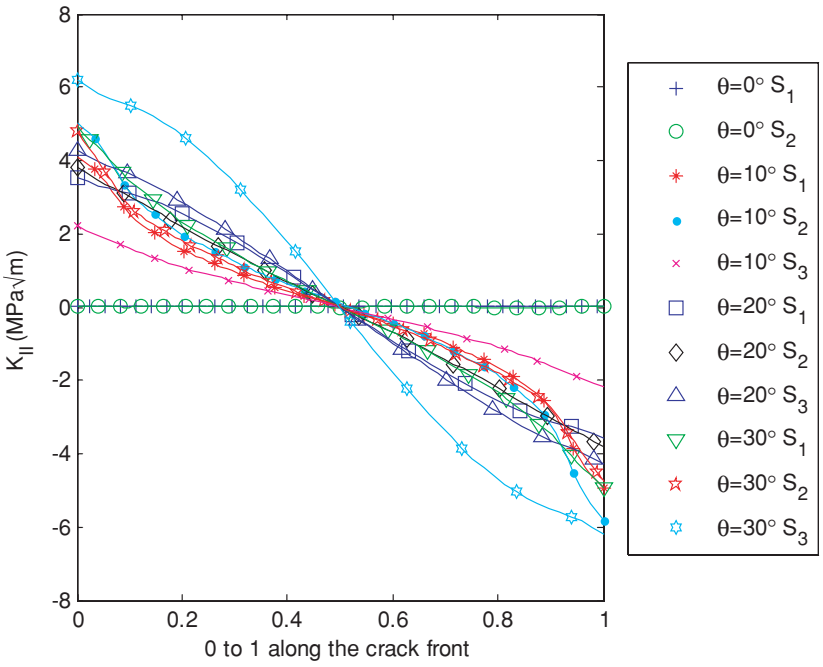

Fig. 8 K_{II} for all analysed specimens as a function of position along the crack front.

the variation of the mixed mode parameters among the experimental samples at the surface, the depth, and where the max value of the parameters is calculated.

MIXED-MODE FRACTURE CRITERIA

Once the SIFs are computed, there are multiple mixed-mode fracture equations that could be used to evaluate an effective mixed-mode fracture parameter. For our analysis, we will rely on equations that have a mechanistic/energy basis rather than the multitude of empirical equations that have been proposed in other works.[1] We investigate four widely used mixed-mode fracture criteria: (i) non-coplanar strain energy release rate (NCSERR) criterion, (ii) maximum normal stress (MNS) criterion, (iii) minimum strain energy density (MSED) criterion, and (iv) critical strain energy release rate (CSERR) criterion.

The NCSERR criterion assumes that the crack growth starts at a critical value of the strain energy release rate and it grows in a direction along which it is maximal.[20]

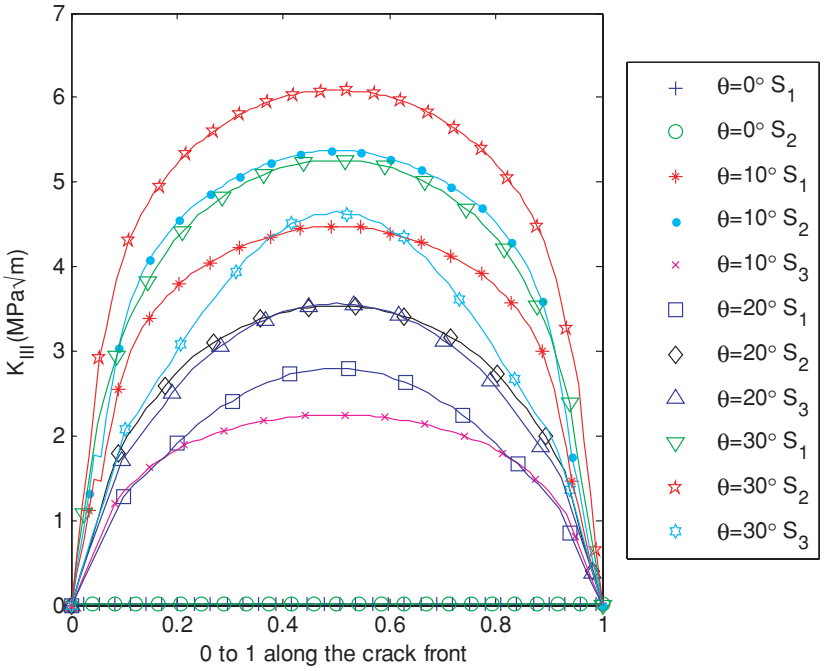

Fig. 9 K_{III} for all analysed specimens as a function of position along the crack front.

Utilizing this methodology the equations for this criterion in the specific case of an angled semi-elliptical flaw have been derived by Qian[1] as:

At point A (see Fig. 6), where the crack meets the specimen surface and $K_{III} = 0$,

$$K_{NCSERR} = \sqrt{\frac{1}{1-v^2}\left(\frac{1}{2}\cos\frac{\gamma}{2}\right)^2 \{[K_I(1+\cos\gamma) - 3K_{II}\sin\gamma]^2 + [K_{II}(3\cos\gamma - 1)]^2\}}. \quad (13)$$

At point B (see Fig. 6), at the crack depth, where $K_{II} = 0$,

$$K_{NCSERR} = \sqrt{K_I^2 + \frac{1}{1-v}K_{III}^2}. \quad (14)$$

Griffith proposed a maximum normal stress (MNS) criterion where fracture nucleates when the maximum stressed point on the surface reaches a specific tensile stress and the direction of the crack growth is normal to it.[21] The fracture condition is given by:[22]

Again, at point A (see Fig. 6), where the crack meets the specimen surface and $K_{III} = 0$,

$$K_{MNS} = \cos\frac{\gamma}{2}\left(K_I\cos^2\frac{\gamma}{2} - \frac{3}{2}K_{II}\sin\gamma\right). \quad (15a)$$

At point B (see Fig. 6), at the crack depth, where $K_{II} = 0$,

$$K_{MNS} = \frac{1}{2}\left[K_I(1+2v) + \sqrt{K_I^2(1-2v)^2 + 4K_{III}^2}\right], \quad (15b)$$

where γ is the angle between the initial crack plane and the plane of propagation (shown in Fig. 1).

Other methods of crack propagation, in mixed-mode conditions, have been proposed with energy considerations. Sih developed a theory based on the strain energy distribution near the crack tip and defined a parameter called the strain energy density factor, S, given by:[1]

$$S = a_{11}K_I^2 + 2a_{12}K_IK_{II} + a_{22}K_{II}^2 + a_{33}K_{III}^2. \quad (16)$$

Sih[23] proposed the minimum strain energy density (MSED) criterion where the crack propagates in a radial direction along which S is minimum and the crack growth starts at a critical value of S.

At point A (see Fig. 6), where the crack meets the specimen surface, for $\eta = (3-v)/1+v$ (plane stress) and $K_{III} = 0$,

$$K_{MSED} = \sqrt{\frac{1}{4(1-2v)}\left\{16\mu a_{11}K_I^2 + 2(16\mu)K_IK_{II}\sin\gamma a_{12} + \left[\frac{4}{1+v}(1-\cos\gamma) + (1+\cos\gamma)(3\cos\gamma - 1)K_{II}^2\right]\right\}}, \quad (17a)$$

where for Poisson's ratio of 0.25,

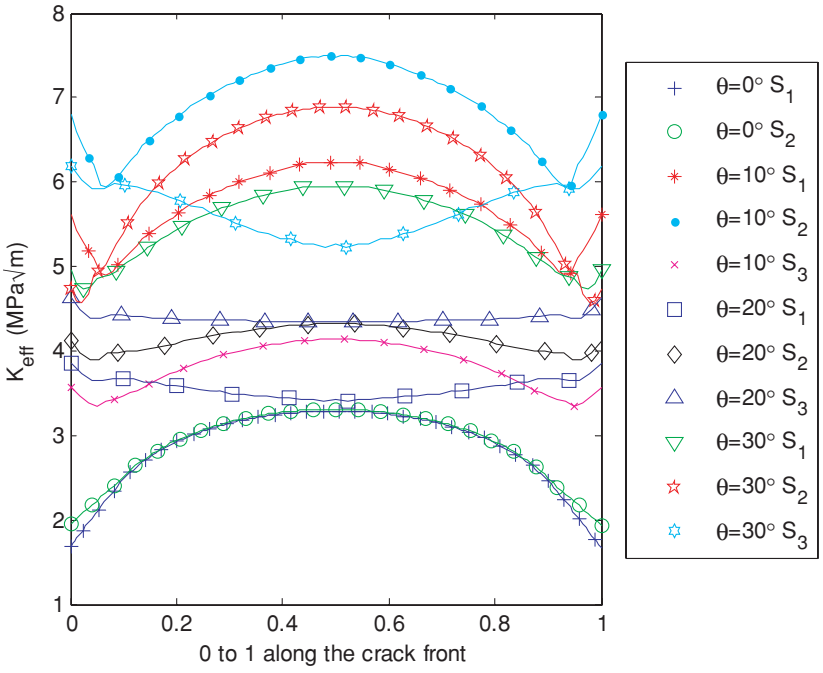

Fig. 10. K_c using the critical strain energy release rate (in the form $K_{GC} = \sqrt{EG_c}$) using K_I, K_{II} and K_{III} as a function of crack front position.

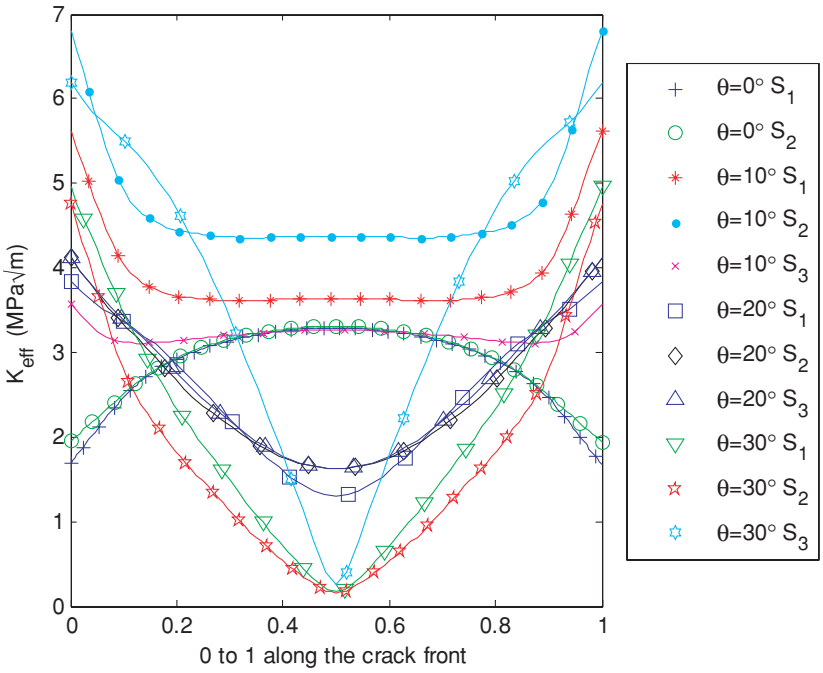

Fig. 11 K_c using the critical strain energy release rate (in the form $K_{GC} = \sqrt{EG_c}$) using K_I and K_{II} as a function of crack front position (K_{III} is neglected).

$$a_{11} = \frac{1}{16\mu}(1+\cos\gamma)(\eta-\cos\gamma) \tag{17b}$$

$$a_{12} = \frac{1}{16\mu}\sin\gamma(2\cos\gamma-(\eta-1)) \tag{17c}$$

$$a_{22} = \frac{1}{16\eta}(\eta+1)(1-\cos\gamma)+(1+\cos\gamma)(3\cos\gamma-1) \tag{17d}$$

$$a_{33} = \frac{1}{4\mu}. \tag{17e}$$

For point B (see Fig. 6), at the crack depth, where $K_{II} = 0$,

$$K_{MSED} = \left[K_{II}^2 + \frac{1}{1-2v}K_{III}^2\right]^{1/2}. \tag{18}$$

Sih's MSED hypothesis is the most accepted theory for failure in mixed-mode loading for brittle materials.[23]

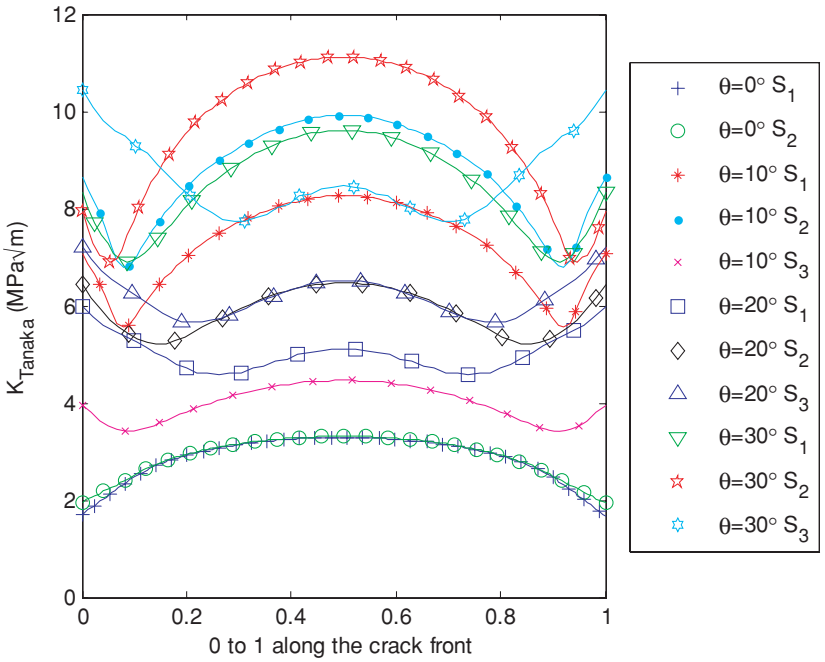

Fig. 12 K_{eff} using Tanaka's relationship of three SIFs as a function of crack front position.

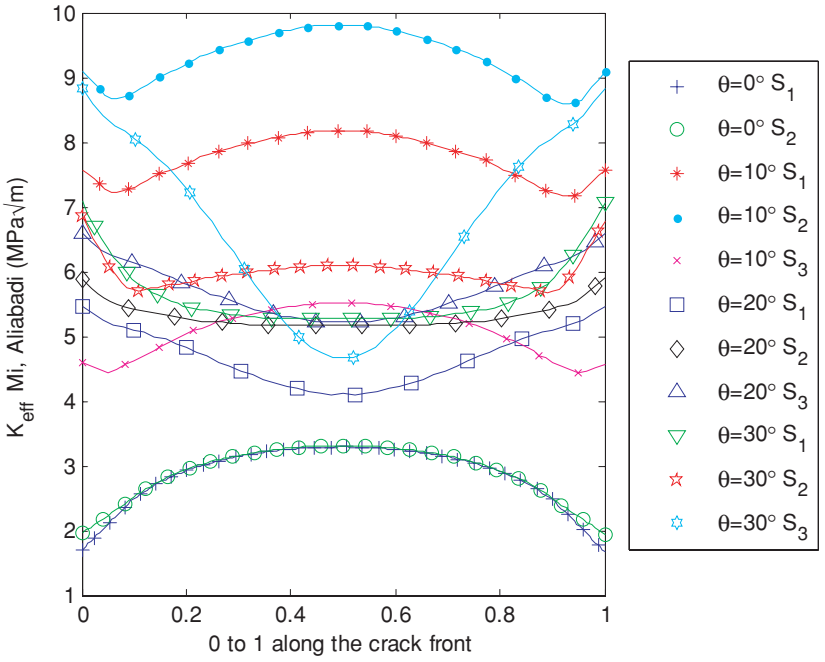

Fig. 13 K_{eff} using Mi and Aliabadi's relationship $K_{\text{eff}} = \sqrt{(K_{\text{I}} + B|K_{\text{III}}|)^2 + K_{\text{II}}^2}$ where $B = 1$ as a function of crack front position.

The fourth fracture criterion used for the calculation of K_C is based on the assumption that the crack starts propagating at a critical value of the strain energy release rate in the same plane as that of the initial crack.[24] The strain energy release rate can be evaluated according to:

$$G = \frac{1}{E}\left(K_{\text{I}}^2 + K_{\text{II}}^2\right) + \frac{1}{2\mu}K_{\text{III}}^2. \tag{19}$$

Knowing the critical strain energy release rate, G_c, a critical SIF can be expressed as:

$$K_{GC} = \sqrt{EG_c}. \tag{20}$$

At point A (see Fig. 6), where the crack meets the specimen surface and $K_{\text{III}} = 0$,

$$K_{GC} = \sqrt{E\left(\frac{1}{E}\left(K_{\mathrm{I}}^{2^2} + K_{\mathrm{II}}^2\right)\right)} = \sqrt{\left(K_{\mathrm{I}}^2 + K_{\mathrm{II}}^2\right)} = K_{\mathrm{I}}\left(1 + \frac{K_{\mathrm{II}}^2}{K_{\mathrm{I}}^2}\right)^{1/2}. \quad (21)$$

For point B (see Fig. 6), at the crack depth, where $K_{\mathrm{II}} = 0$,

$$K_{GC} = \sqrt{E\left(\frac{K_{\mathrm{I}}^2}{E} + \frac{K_{\mathrm{III}}^2}{2\mu}\right)} = \sqrt{\left(K_{\mathrm{I}}^2 + \frac{K_{\mathrm{III}}^2}{2(1+\upsilon)}\right)}. \quad (22)$$

For comparison, we are also including empirical equations from mixed-mode fatigue analyses. Tanaka investigated effects of mixed mode fatigue for aluminium sheets with angled cracks at $R = 0.65$ and derived the fatigue crack growth law based on the effective SIF given by[25]

$$K_{\mathrm{eff}} = \left(K_{\mathrm{I}}^4 + 8K_{\mathrm{II}}^4 + 8\frac{1}{1-v}K_{\mathrm{III}}^4\right)^{1/4}. \quad (23)$$

From Mi and Aliabadi we have mixed mode effective fatigue SIF as,[26]

$$K_{\mathrm{eff}} = \sqrt{(K_{\mathrm{I}} + B|K_{\mathrm{III}}|)^2 + K_{\mathrm{II}}^2}. \quad (24)$$

ANALYSIS

The most effective mixed mode criteria will be identified based on analysing each of the theories by using SIFs that are calculated as a function of position along the surface crack front, using the SIFs computed along the crack front. Previous work on BD specimens has investigated through thickness cracks based on two-dimensional plane stress solutions that provide a single value of K_{I} and K_{II} at the crack tip. Here the semi-elliptical surface flaw has only K_{I} for the vertical crack ($\theta = 0$) but has all three modes present along the crack front as the crack becomes inclined to the load axis. The mixed mode fracture criteria highlighted in Eqs (13–15, 17–18, 21–22) can be evaluated as a function of crack position, using the SIFs evaluated via FEA (see Table 2). We would like to identify the location along the crack front where these criteria reach maximum values.

It is difficult to establish the precise location along the crack front where fracture initiates by examination of the fracture surface (see Fig. 1). We can reasonably expect that fracture initiates at a point along the crack front where the effective fracture parameter reaches a maximum value. We have established from 3D FEA results that the maxima of the SIFs occur at either where the crack meets the surface (point A in Fig. 6) or at the depth of the crack (point B in Fig. 6).[24] As a result, we can calculate the mixed-mode fracture (see Figs 10–13) criteria outlined at the depth, at the surface, and the maximum value along the crack front. Table 2 lists the K_{I}, $K_{\mathrm{I}}^{\mathrm{Resid}}$, $K_{\mathrm{I}}^{\mathrm{Total}}$, K_{II} and the four fracture criteria calculated at the surface (point A in Fig. 6) and crack depth (point B in Fig. 6). Properties of brittle materials inherently have higher variability arising from sensitivity to defect distributions. Fracture properties of silicon nitride, made from powder compaction, is particularly sensitive to processing variables. In order to identify the most effective mixed-mode fracture parameter, we calculate the standard deviation between each of the 11 samples that were fractured. In Table 3, we have the averages and standard deviations between all samples at the surface (point A in Fig. 6), at the crack depth (point B in Fig. 6), and maximum value along the crack front, for each fracture criteria. In comparing these we find the following (in MPa$\sqrt{}$m) with increasing standard deviations: CSERR = 5.00 ± 1.29, NCSERR = 5.89 ± 1.31, MSE = 6.72 ± 1.47, and MNS = 7.04 ± 1.59. The fatigue criteria by Mi and Aliabadi[26] yielded 7.57 ± 1.28 and 7.55 ± 2.29 for Tanaka.[25] The fatigue criteria are empirical and were designed for metallic materials and yield high mean fracture toughness values for silicon nitride along with higher standard deviation.

Table 2 K_c values in MPa$\sqrt{}$m for point A, using FEA computed SIFs and an experimentally measured turning angle for specific specimen/flaw geometries and orientations as tested experimentally

	K_{I}	$K_{\mathrm{I}}^{\mathrm{resid}}$	$K_{\mathrm{I}}^{\mathrm{Total}}$	K_{II}	K_{NCSERR}	K_{MNS}	K_{MSE}	K_{CSERR}
$\theta = 0^\circ$ S_1	3.30	1.40	4.70	0.00	4.70	4.70	4.70	4.70
$\theta = 0^\circ$ S_2	3.31	1.40	4.71	0.00	4.71	4.71	4.71	4.71
$\theta = 10^\circ$ S_1	3.55	1.40	4.95	4.00	7.27	6.41	7.42	6.61
$\theta = 10^\circ$ S_2	3.67	1.40	5.07	4.78	8.01	7.00	7.40	6.85
$\theta = 10^\circ$ S_3	3.27	1.40	4.67	2.22	5.35	5.06	4.95	4.85
$\theta = 20^\circ$ S_1	1.48	1.40	2.88	3.58	5.85	4.96	4.85	4.60
$\theta = 20^\circ$ S_2	1.61	1.40	3.01	3.84	6.33	5.37	5.05	4.88
$\theta = 20^\circ$ S_3	1.79	1.40	3.19	4.32	6.45	5.22	6.11	5.35
$\theta = 30^\circ$ S_1	0.00	1.40	1.40	5.00	5.68	3.52	6.35	4.90
$\theta = 30^\circ$ S_2	0.00	1.40	1.40	4.76	5.83	3.53	5.90	4.89
$\theta = 30^\circ$ S_3	0.00	1.40	1.40	6.22	8.36	6.15	6.67	6.10

Table 3 The mean K_c values in MPa$\sqrt{}$m calculated for each method with the standard deviation

Location	K_{NCESR}	K_{MNS}	K_{MSE}	K_{GC}	K_{TAN}	K_{Mi}
Max	5.89 ± 1.31	7.04 ± 1.59	6.72 ± 1.47	5.00 ± 1.29	7.55 ± 2.29	7.57 ± 1.28
Surface ($K_{III} = 0$)	4.96 ± 1.79	2.25 ± 3.08	6.61 ± 1.57	4.45 ± 1.38	6.67 ± 2.09	7.04 ± 1.32
Depth ($K_{II} = 0$)	5.72 ± 1.13	6.20 ± 1.35	6.67 ± 1.63	4.83 ± 1.31	7.14 ± 2.15	6.89 ± 1.49

We note that CSERR criterion yields the lowest standard deviation and the mean fracture toughness agrees well with recently published results for silicon nitride. The NCSERR criterion also yields rather similar results. Fracture toughness results from Piotrowski and O'Brien[3] for silicon nitride is 4.85 ± 0.36 MPa$\sqrt{}$m, using a Vickers indented half-inch diameter ball in diametral compression in pure mode I loading. The indentation fracture toughness for the same material is 5.48 ± 1.34 MPa$\sqrt{}$m. Indentation fracture toughness tends to have higher variability because of the assumption that Vickers indentation produces perfect semi-circular cracks.[27] We have used multiple collinear closely spaced Vickers indents that link up to produce a long semi-elliptical surface flaw. This is shown on the fracture surface of Fig. 1. The cracks linking up in this fashion was not as easily observed on all specimens and the variation in these linking trends can lead to variation in the measured flaw size and hence fracture toughness results. We note that for the two samples fractured at $\theta = 0^\circ$ (pure mode I condition) K_I values evaluated are very close. The variability observed is higher for mixed-mode loading. If the inherent material variability is constant (because all disc specimens came from the same batch processed identically), then mixed mode fracture properties of silicon nitride shows higher variability than mode I fracture. These trends need to be further verified by larger sample size.

As an input FEA requires the specimen dimensions, load at fracture, and initial surface crack dimensions. The specimen dimension is well defined and has negligible error. The load at fracture is measured by the load frame and its error is also quite negligible. The largest source of error comes from the crack dimensions which are determined by examining the fracture surface after specimen failure, as shown in Fig. 1. Our experimental procedures suggest that an average error of crack depth measurement is on the order of 50 μm. This error stems largely from uncertainty in locating the crack front. The resulting error in the SIFs would be:

$$K = \sigma\sqrt{\pi a} \Rightarrow \%\text{Error in } K = \frac{1}{2}\left(\frac{\Delta a}{a}\right) \times 100\% = \frac{1}{2}\left(\frac{50\,\mu\text{m}}{a}\right) \times 100\%. \quad (25)$$

Looking at Table 1, for $a = 190$–490 μm, a range of error in the stress intensity factors can be between ± 5.1 and $\pm 13.2\%$ which translates into ± 0.26 to ± 0.66 MPa$\sqrt{}$m of the calculated 5.00 ± 1.29 MPa$\sqrt{}$m by the CSERR criterion.

RESULTS AND DISCUSSION

Stress intensity factors were calculated for each experimental study by simulating the measured crack dimensions under the load that induced failure (see Table 1). The SIFs were combined into each mixed-mode fracture criterion (see Table 2) and the averages and standard deviations of each are shown (see Table 3). The mixed mode parameters are tabulated for the maximal values along the front, at the depth of the crack and where the crack meets the surface of the specimen. We tabulated the surface values separately because this is where the angle of crack growth, γ, was measured on the experimental specimens. Also, at this location $K_{III} = 0$ which simplifies our effective K_c calculations. In addition, some experimental observations have indicated that this is the point where fracture is likely to initiate.

Due to the geometry of the experiment, as the angle of the crack increases, K_I decreases while K_{II} and K_{III} increase. K_{Ic} is measured for $\theta = 0^\circ$ specimens (as 3.30 and 3.31 MPa$\sqrt{}$m SIF computed was for the S1 and S2 specimens by FEA, as seen in Table 2, and when superposed with the 1.40 MPa$\sqrt{}$m from residual stress by the Vickers indent we get 4.70 and 4.71 MPa$\sqrt{}$m) and is close to the 4.85 ± 0.36 MPa$\sqrt{}$m mode I fracture toughness reported by Piotrowski and O'Brien[3] for silicon nitride. Pure K_I loading results in the smallest calculated K_c parameter, but with K_{II} and K_{III} contribution the mixed-mode K_c ends up at an average 5.00 ± 1.29 MPa$\sqrt{}$m (whose error is the calculated standard deviation among tests).

Figure 3 shows the fractured specimens as a function of the angle θ. The fracture of the specimen at $\theta = 0^\circ$, which consisted entirely of pure mode I lodaing, occurred along the initial plane of the flaw. However at all other angles, the crack deviated from its initial plane. At the same time, it can be noticed that the inclined crack deviates from its initial plane to propagate in a direction normal to the maximum principal stress. It was also seen that in some of the samples, the cracks did not encompass all the Vickers indents on the sample. The disk shattered to several pieces at $\theta = 35^\circ$ and at $\theta = 40^\circ$ (see Fig. 3c). Crack closure at

these angles is the most reasonable explanation for this observation and was demonstrated in 3D FE models also. Because the disc centre crack could not propagate due to closure, the disc shattered with increasing load, with crack growth initiating at the load support due to high contact stress.

SUMMARY

A detailed numerical and experimental investigation of mixed-mode fracture toughness of NBD300 silicon nitride material is presented based on the Brazilian disc test. The results from the investigation are summarized below:

1 The Brazilian disc test was conducted on thirteen NBD300 circular discs which were centrally pre-cracked using Vickers indentation, to generate a semi-elliptical surface flaw and loaded at a range of mode-mixities/crack angles, until fracture.
2 Three-dimensional FEA was used to compute all three modes of stress intensity factors, along the crack front, present at the point of fracture.
3 Using experimental data and numerical modelling four mixed-mode fracture criteria are investigated, namely, (i) non-coplanar strain energy release rate criterion, (ii) maximum normal stress criterion, (iii) minimum strain energy density criterion and (iv) critical strain energy release rate criterion.
4 The effective mixed-mode fracture toughness for silicon nitride is determined based on evaluating four different mixed-mode fracture criteria.
5 The critical strain energy release rate (CSERR) criterion is deemed the simplest and the most effective mixed-mode fracture criteria to implement, based on its standard deviation being lowest compared to methods investigated. The predicted mixed-mode fracture toughness for the NBD300 silicon nitride tested is 5.00 ± 1.29 MPa$\sqrt{\text{m}}$.

Acknowledgement

The Timken Company, Canton, OH, supported this work through the U.S. Air Force/VAATE Contract #: F33615-03-D-2353-003. We thank Robert Wolfe of the Timken Company for providing us with the silicon nitride BD specimens.

REFERENCES

1 Qian, J. and Fatemi, A. (1996) Mixed mode fatigue crack growth: a literature survey. *Eng. Fract. Mech.* **55,** 969–990.
2 Carneiro, F. L. L. and Barcellos, A. (1953) Tensile strength of concrete. *RILEM Bulletin.* **13,** 97–123.
3 Piotrowski, A. E. and O'Brien, M.J. (2006) A novel test method to measure the fracture toughness of ceramic balls used in bearings. *Fatigue Fracture Eng. Mater. Struct.* **29,** 558–572.
4 Bank-Sills, L., Travitzky, N., Ashkenazi, D. and Eliasi, R. (1999) A methodology for measuring interface fracture properties of composite materials. *Int. J. Fract.* **99,** 143–161.
5 Zhou, J., Wang, Y. and Xia, Y. (2006) Mode-I fracture toughness measurement of PMMA with the Brazilian disk test. *J. Mater. Sci.* **41,** 5778–5781.
6 Tong, J., Wong, K. Y. and Lupton, C. (2007) Determination of interfacial fracture toughness of bone-cement interface using sandwich Brazilian disks. *Eng. Fract. Mech.* **74,** 1904–1916.
7 Awajiand, H., and Sato, S. (1978) Combined mode fracture toughness measurement by the disk test. *J. Eng. Mater. Tech.* **100,** 175–182.
8 Petrovic, J.J. and Mendiratta, M. G. (1976) Mixed-mode fracture from controlled surface flaws in hot pressed silicon nitride. *J. Am. Ceram. Soc.* **59,** 163–167.
9 Khandelwal, P., Majumdar, B. S. and Rosenfield, A. R. (1995) Mixed-mode high temperature toughness of silicon nitride. *J. Mater. Sci.* **30,** 395–398.
10 Jahanmir, S. (1994) *Friction and Wear of Ceramics*. Marcel Dekker, Inc., New York, Basel, Hong Kong.
11 Levesque, G. and Arakere, N. K. (2008) An investigation of partial cone cracks in silicon nitride balls. *Int. J. Solids Struct.* **45,** 6301–6315.
12 Wang, Y. (2000) Failure modes of silicon nitride rolling elements with ring cracks. PhD Thesis, Bournemouth University, UK.
13 Marshall, D. B., Lawn, B. R. and Mecholsky, J.J. (1980) Effect of Residual Contact stresses on Mirror/Flaw Size Relation. *J. Am. Ceram. Soc.* **63,** 358–360.
14 Mitchell, N. B. (October 1961) The indirect tension for concrete. *Materials Research and Standards*, ASTM, pp. 780–788.
15 Hibbet, Karlsson, Sorensen, SIMULIA, ABAQUS Theory Manual. v6.7.1 Providence, RI.
16 Banks-Sills, L., Hershkovitz, I., Wawrzynek, P. A., Eliasi, R. and Ingraffea, A. R. (2005) Methods for calculating stress intensity factors in anisotropic materials: Part I– z = 0 is a symmetric plane. *Eng. Fract. Mech.* **72,** 2328–2358.
17 Lawn, B. (1993) *Fracture of Brittle Solids*. Cambridge University Press, Cambridge, UK.
18 Anstis, G. R., Chantikul, P., Lawn, B. R. and Marshall, D. B. (1981) A critical evaluation of indentation techniques for measuring fracture toughness: I, direct crack mechanisms. *J. Am. Ceram. Soc.* **64,** 533–538.
19 Jayatilaka, Ayal de S. (1979) *Fracture of Engineering Brittle Materials*. Applied Science Publishers Ltd., pp. 90–107.
20 Hussain, M.A., Pu, S. L. and Underwood, J. (1974), A.S.T.M. STP. London, UK. *Fract. Anal.* **560,** 2–28.
21 Griffith, A. A. (1920) The phenomena of rupture and flow in solids. *Philos. Trans., Ser. A* **221,** 163–198.
22 Sih, G. C. (1974) Strain-energy density factor applied to mixed-mode crack problems. *Int. J. Fract.* **10,** 305–331.
23 Erdogan, F. and Sih, G. C. (1963) Crack extension in plates under plane loading and transverse shear. *J. Basic Eng. Trans. A.S.M.E., Ser. D.* **85,** 519–527.

24 Chen, X. M., Jiao, G. Q. and Cui, Z.Y. (1986) Application of combined-mode fracture criteria to surface crack problems. *Eng. Fract. Mech.* **24,** 127–144.
25 Tanaka, K. (1996) fatigue propagation from a crack inclined to the cyclic tensile axis. *Eng. Fract. Mech.* **55,** 969.
26 Mi, Y. and Aliabadi, M. H. (1995) An automatic procedure for mixed-mode crack-growth analysis. *Commun. Numer. Meth. Engng.* **11,** 167–177.
27 Smithand, S. M. and Scattergood, R. O. (1992) Crack-shape effects for indentation fracture toughness measurements. *J. Am. Ceram. Soc.* **75,** 305–315.